5.2   Wing Section Prototyping

Based on the results obtained by CFD simulation the wing section prototype has been designed and manufactured. The schematic, reported in Figure 5.7, shows the overall architecture designed to be prototyped. The geometrical characteristics are:

- Wing section chord length: 0.2 (m);

- Wing section spanwise: 0.3 (m) ;

- Wing section airfoil: NACA 0024.

The materials' choice is made for structural solidity requirements during LCOs, and for finding appropriate accommodation of the solenoidal actuators. In particular, twenty wooden made wing sections are the inner structure of the wing prototype. They are $1(cm)$ thick, properly milled, lightened and cut to host the actuation system, as shown in Figure 5.8. Wood has been chosen because of its structural properties, cost and ease of processing. The small wing sections, once polished, are glued and held together by two aluminum bars, located at 20% and 80% of the chord length. The bars are threaded at the tip to obtain compression by tightening the flat bolts acting on the external wing sections. The actuation system is embedded in the wing model. It is composed by push type solenoids, where the strokes acts on an aluminum plate, that is the actual spoiler. When the solenoid is powered it pushes out the stroke deflecting the spoiler at $85(deg)$. The spoiler is realized by two hinged aluminum plates, one of which is glued to the wing surface and the other is free to rotate. A small return spring guarantees closure motion when the solenoid is not powered. The spoiler hinge is located to comply with the CFD optimization process results. It is embedded in the wing surface by an appropriate groove. The wooden wing surface is treated with a thin layer of plaster (white color in Figure 5.8) and then covered by a monokote film (black color in Figure 5.9). This components are employed to guarantee the correct airfoil shape and a low level of surface roughness. When fully deployed the five spoilers operate across the entire wing section span. However, as the control action required is not always maximal, a pre-defined coordinated opening strategy has been implemented. The strategy is intended to preserve pressure distribution symmetry on the wing upper surface, so as to avoid undesirable rolling moment. Numbering the spoilers progressively, 1 to 5, from left to right along the wing section span, the opening strategy sequence is: spoiler #3, #2-4, #1-3-5,#1-2-4-5 and finally #1-2-3-4-5. The solenoid actuation works at $5(Volt)$. The final prototype is shown in Figure 5.9 during wind tunnel static tests. The predefined opening strategy is realized by implementing a
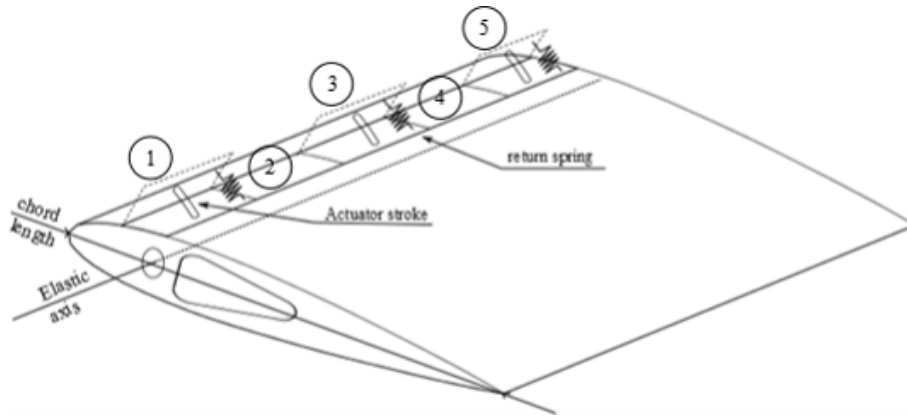
Figure 5.7: Wing-Spoiler configuration, prototype schematic.

control algorithm on an Arduino board, which is used both for sensing and controlling, as it will be explained on section 5.5 in the aeroelastic dynamic experiment. The actuators are wired to a custom made electric board with optical diode, which serves as protection bridge to avoid the higher current, supplying them, to flow back to the Arduino board. The electric wires runs inside the wing and are places to minimize the interference with the wing section aerodynamics during wind tunnel test.

5.3 Wind Tunnel Static Test

A wind tunnel static test campaign is conducted primarily to verify and validate the results obtained with the CFD optimization. In addition, the aerodynamic database derived from the tests serve to implement a realistic mathematical model to allow control law design for real time application of LCO suppression. The experiment setup and wing configuration are shown in Figure 5.10. A couple of changes were required on the proto-typed wing section to accomplish the test. First, part of the material has been properly removed to accommodate the balance stinger and to guar-antee solid connection for sensing accuracy. Second, the wing section has been provided by Plexiglas end-plates, screwed to the tip with a intersti-tial foam for vibration reduction. Both configurations, with and without end-plates, are tested to evaluate three-dimensional aerodynamic effect. 2D configuration is employed to validate CFD results and 3D configuration for control law design purpose, because the end-plates are not included during the aeroelastic dynamic tests. The experimental campaign is conducted at Clarkson Universitys high-speed (CUHS) wind tunnel test facility, shown in Figure 5.11. It is an open-circuit eiffel-type wind tunnel capable of pro-ducing wind speeds up to 70 m/s in the test section. Turbulence level is controlled with one honeycomb and two conditioning screens included in

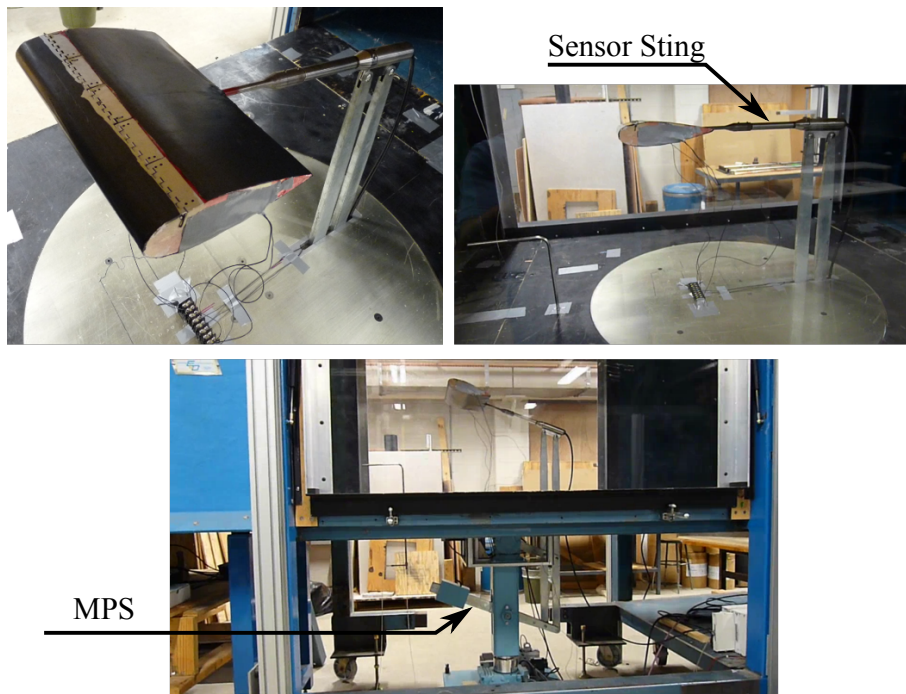Figure 5.8: Wing-Spoiler configuration, prototype characteristic.

Figure 5.9: Final prototype and wind tunnel static experiment setup.

the settling chamber. The tunnel has a test section of $48 \times 36 \times 60(inches)$, that are $1.2192 \times 0.9144 \times 1.524(meter)$.The floor and ceiling are made of medium density fiber wood. The sidewalls are made of clear Plexiglas to allow optical access for visualization. The contraction ratio is 8:1. The tunnel is powered by a 179 hp electro-motor and is controlled by an ABB (model: ACS550-U1-180A-4) industrial controller. Previous investigations [93] demonstrate that the turbulence intensity, in the vertical and horizontal directions, was approximately 1.8%. Sensors of temperature, relative humidity and the atmospheric pressure are available for actual density calculation during the experiment. The pitot-static tube, for airflow speed monitoring, is placed upstream the model at the beginning of the test section, with an optimized location to reduce interference with the model. The sensor is connected to a Mensor digital gauge model 2500. An $18 \times 8(inches)$, that is $0.457 \times 0.203(m)$, acrylic window, placed in the test section ceiling is used to place the aeroelastic apparatus on top of the ceiling, outside the test section to avoid aerodynamic interference with the aeroelastic experiment. The force balance, produced by *Aerolab, Inc.*, is provided with a Model Positioning System (MPS) that allows for pitch and yaw control of the model using stepper motors and motor controllers. The motors motion is transfered to the model through two vertical arms to whom the force balance is connected. A LabView virtual instrument is used to control the motors during experiments, Figure 5.12.

5.4 2 DOF Aeroelastic Apparatus: Design and Build

An existing 2 DOF plunging/pitching aeroelastic apparatus has been modified to reproduce LCOs with the prototyped wing section and to test the novel spoiler control architecture. It has been previously developed at Clarkson University for energy harvesting research purpose and is described in [94]. The apparatus, shown in 5.13, is made of an industrial carriage and guide rail system (*Techno-Isel*) to minimize frictional losses and unknown system damping in the plunging motion. The carriage has four grooved roller bearings that allow for various pre-load conditions with adjustable eccentricity. in this application they were set up by hand for no free-play and minimal pre-load. An aluminum circular flange, equipped with two rolling bearings, is installed in the carriage center and hold the wing elastic axis, allowing only rotary motion. Two posts are placed in the carriage corner for the adjustable pitch spring preload mechanism. The aluminum elastic axis is connected to a nonlinear cam that consists of a 2 diameter aluminum disk with a shaft bore located 0.5 eccentrically from the center. Two cams mount adjacent to each other with a setscrew clamping the cam to the 3/8 airfoil shaft. Cables ride in grooves along the outer edge of the cams and
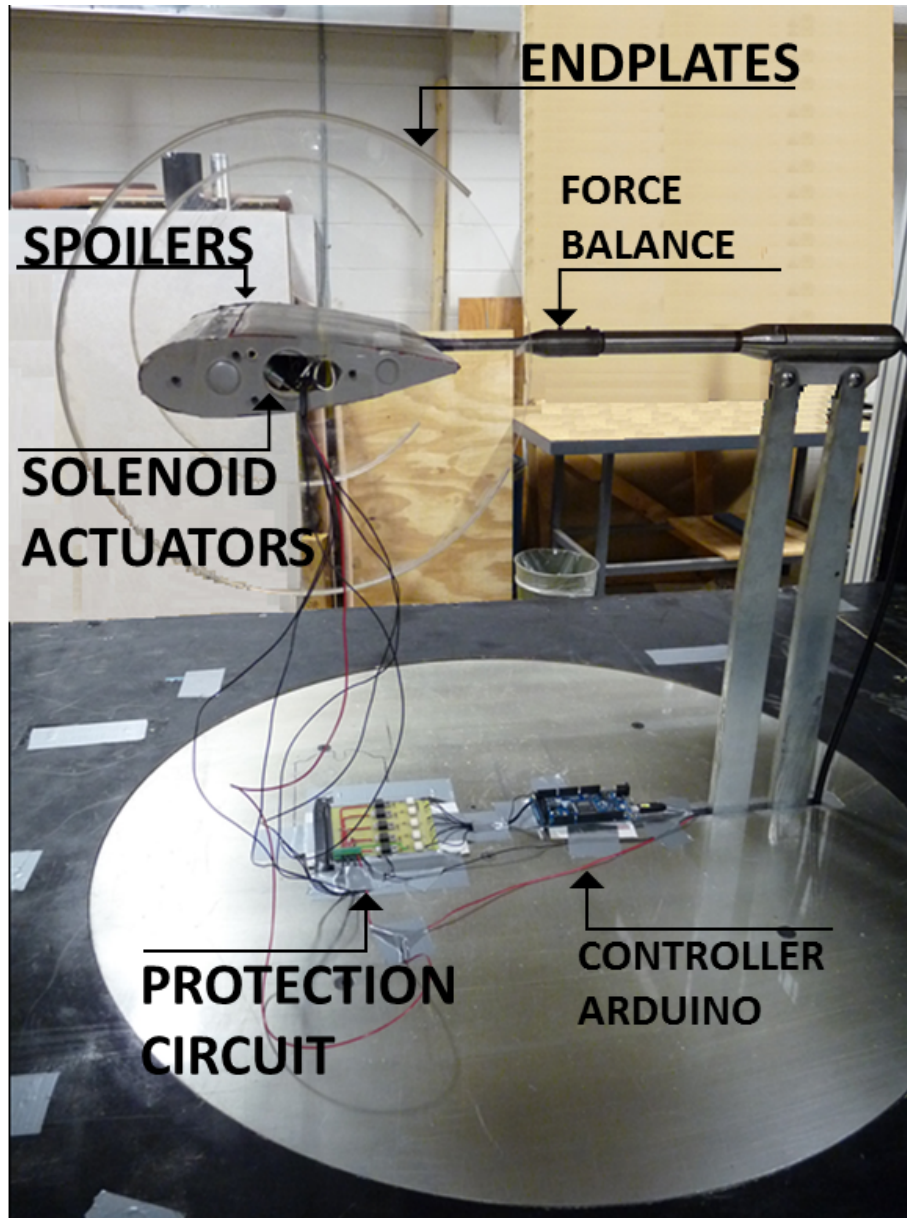
Figure 5.10: Wing-Spoiler configuration, final prototype during wind tunnel testing.

Figure 5.11: Clarkson University Wind Tunnel

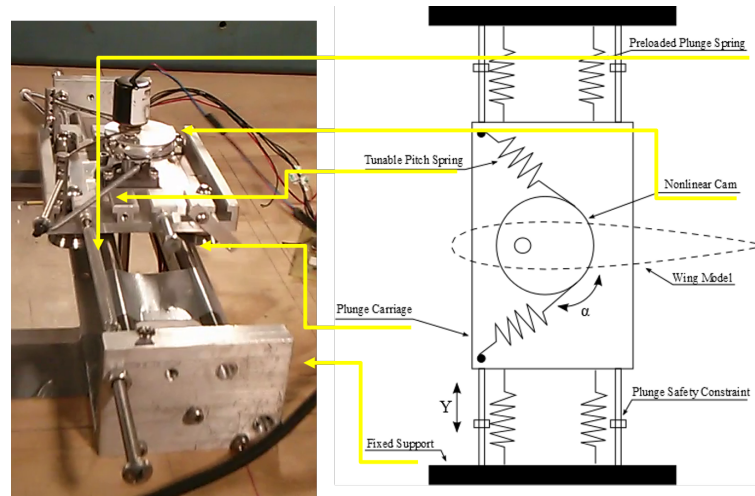Figure 5.12: Clarkson University, Force/Moment Sting Balance and Model Positioning System

Figure 5.13: 2 DOF plunging/pitching aeroelastic apparatus: schematic

connect to pitch springs providing continuous pitch stiffness non-linearity. The stiffness in plunge also has nonlinearity due to spring pre-load. When the plunging carriage is in its central position, there is usually some extension δ_h of the plunge springs compared to their unstretched length. Initial deflection is adjustable by threaded bolts attaching the springs to the side frame. The wing section is connected to the apparatus with the aluminum bar that runs inside the wing at the elastic axis position.

5.5   Dynamic Test Experimental Setup

Dynamic tests have been performed by properly mounting the apparatus described in section 5.4 in the wind tunnel test chamber. The rail-carriage system is screwed on top the wood chamber ceiling, so as to not interfere with the airfoil and to let the wing section laying in vertical position. This solution serves to cancel out any gravitational force component in the LCO regime exhibition. In this configuration the wing oscillates in a right-left motion instead of the typical up-down motion that happens when the carriage mechanisms is mounted on the chamber sidewalls. To accomplish the dynamic test, the overall apparatus is equipped with a sensing and a control system. The controller architecture is made up by the spoilers-solenoids-springs system and will be separately discussed in 5.2. To monitor the system states during experiment the apparatus is provided with two analog sensors:

- A Rotary Variable Inductance Transducer (RVIT) employed for angular position (pitch, α) sensing and shown in 5.14 (area number 1).
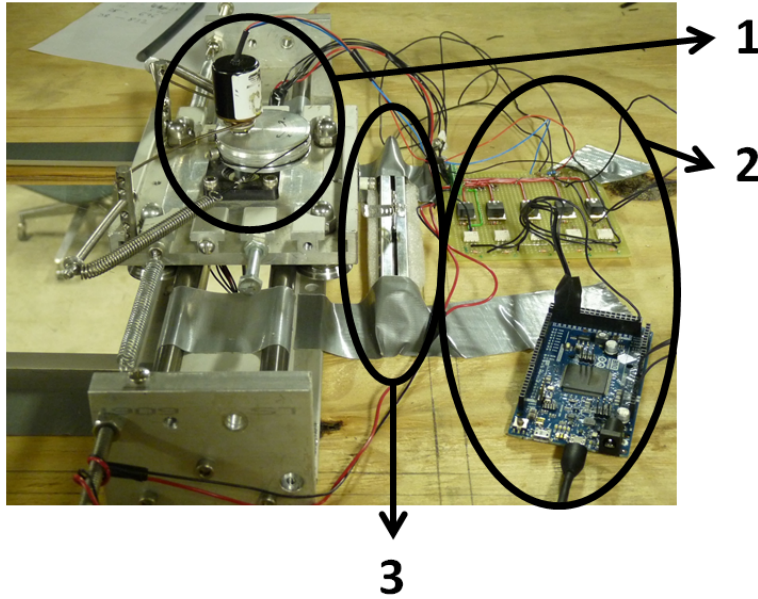
Figure 5.14: 2 DOF apparatus, mounted and in the hardware in the loop configuration

- A linear potentiometer employed for displacement measurement (plunge, h) and shown in 5.14 (area number 3).

The RVIT is the *Schaevitz R120LC*, with 99% linearity, and a $\pm 60 (deg)$ range, and is linked to the elastic axis. The linear sensor is an *ALPS*, low-profile master type (Slim Type) RSN11S Series, and its vertical flange is directly connected to the carriage. The analog signals of the sensors are digitalized by Arduino Duo board after signal conditioning. In this system, 2 of the analog ports of Arduino board are used, which provides 12 bit A/D conversion on both channels.

The measurement and data acquisition system, in the hardware in the loop configuration, receive and convert the data of the angular and linear position sensors, provide the data to the software component (e.g. the control law implemented in Simulink) running in the host computer and save all of the incoming data for post-processing. The data acquisition system consist of:

- Pitch and plunge sensors;

- Arduino Due board;

- Power switching board, area 2 in 5.14;

- Personal Computer.

The Arduino Due board has been programmed so to let the system being fully observable and controllable. The flowchart of the program uploaded into the board is shown in **??**. The employed delays set the time of the main cycle to 20 ms, which means a sample frequency of 50 Hz. The Arduino board is connected to the PC by a USB cable through a VCP port, which gives full duplex serial communication line at 19200 bps. Each data packet is as in 5.16. Arduino board always sends 9 bytes in a data package. The first 4 bytes contain the angular sensor data, the 5th byte holds feedback information about the actual state of the spoilers and the last 4 bytes contain the linear sensor data. The command sent to Arduino is only one byte. This can be sent by any software which the Arduino can be connected to. Since the communication is full duplex, which means sending and receiving can be performed in the same time, it is not required to synchronize the sending and the receiving. The value of the command byte are set as follows:

- 0:   close all spoilers;

- 0-5:   open appropriate number of spoilers;

- 11-15:   open appropriate number of spoilers (only one spoiler);

- 21-25:   close appropriate number of spoilers (only one spoiler);

When command sent is between 1 and 5, the number of open spoilers follows the predefined strategy described in 5.2.

The power switching board is custom made. It is used to provide proper power to the solenoid actuator and the circuit of one channel (five total, one per spoiler) is shown in 5.17. Each solenoid needs 0.5 Amperes near 12 Volts, which cannot be provided by digital port of a microcontroller. To avoid any noise flowing back from the solenoids to the microcontroller, the solenoids and the higher voltage parts are isolated from digital electronic by using optical isolators in each channel. It was also critical, to protect the circuit from electrical impulses generated by solenoids when they are switched off. To this purpose, the protection element is a diode connected in parallel with the solenoid.

The personal computer is used to monitor and control the system through a Simulink code, implemented on purpose. The receiving code section is reported in 5.18. As already explained, 9 bytes are transferred on serial line every cycle. However, the command on the serial line is not sent every cycle but only if the state of spoilers has to be updated. Based on the signal bytes order defined, some lookup tables are required in the Simulink code for the pitch and plunge value conversion. The lookup tables' values are obtained by a sensor calibration process. The overall aeroelastic test architecture is schematically presented in 5.14.
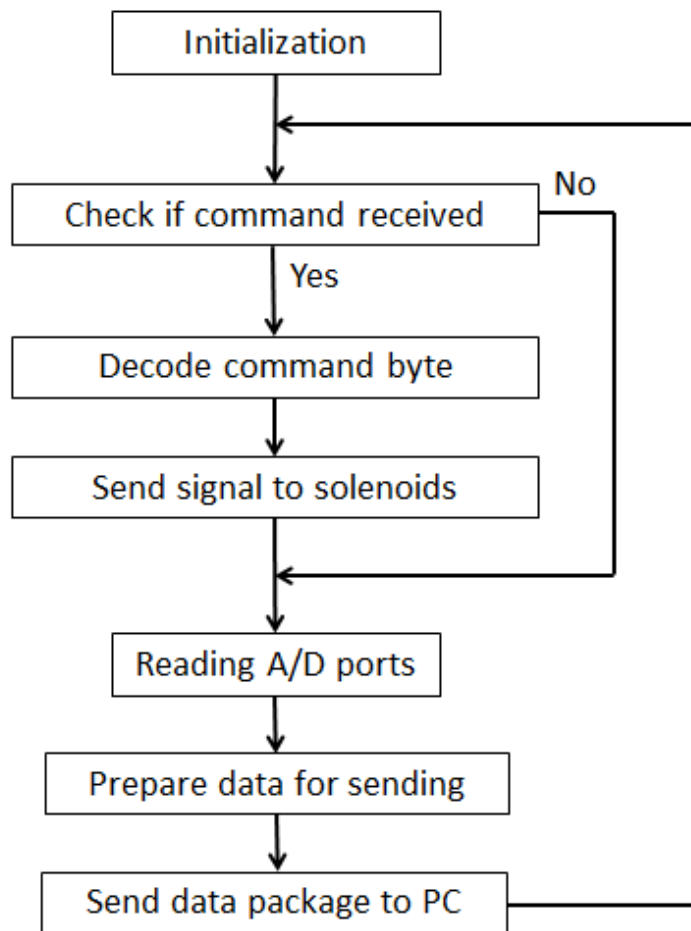
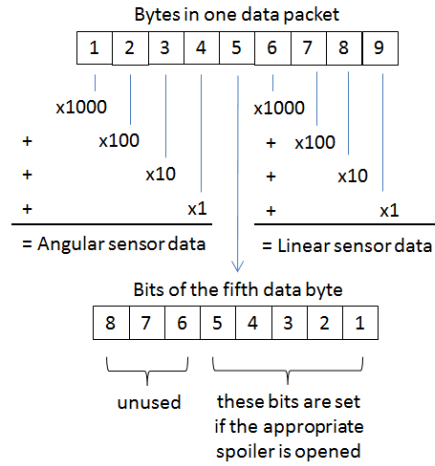Figure 5.15: Implemented program on Arduino Due, flowchart
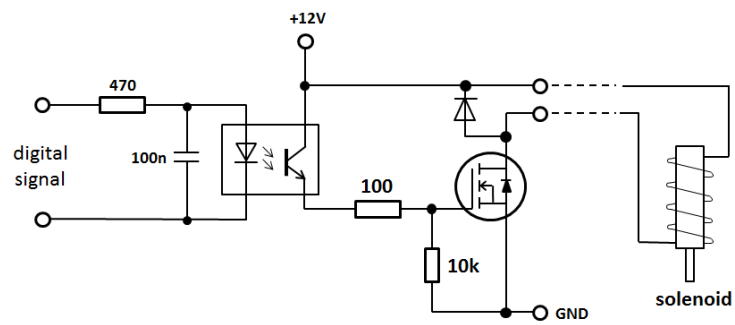
Figure 5.16: Arduino data package description

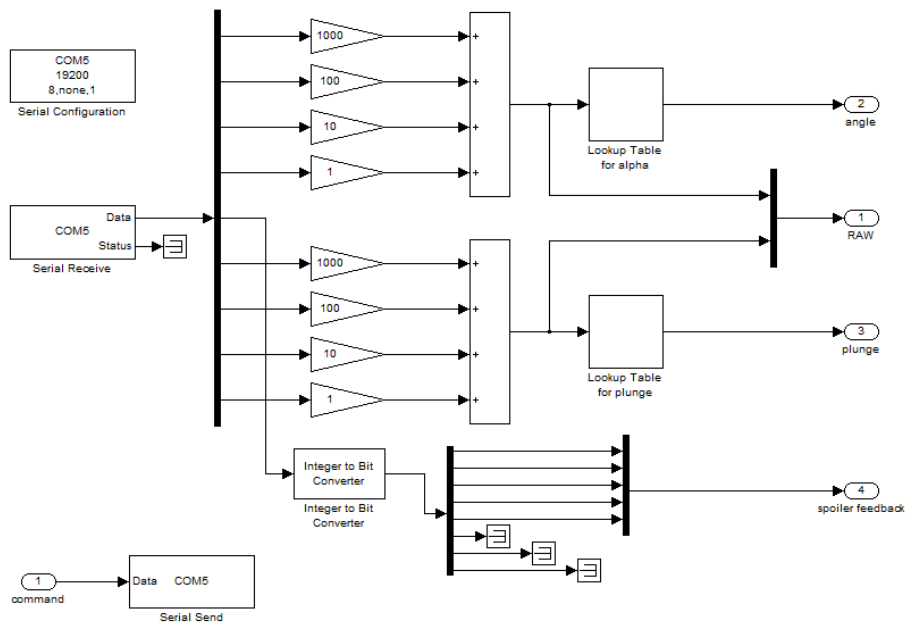Figure 5.17: Power switching board, one channel circuit

Figure 5.18: Simulink code to receive Arduino signal

Figure 5.19: Experimental setup overall architecture schematic

Chapter 6

Experiment Procedure and Results

In this chapter both static and dynamic test procedures and results are presented and discussed. The two type of tests are profoundly different, in the targeted goals as well as in the apparatus and devices employed and so forth in the related issues. For these reasons the chapter is organized in three section, one for each test accomplished. In section 6.1 the wind tunnel six-axis balance measurement procedure and results are illustrated, with particular attention to the aerodynamic coefficient computation. The aerodynamic database already presented in chapter 2 is herein repeated for the sake of completeness. In section 6.2 a detailed description on the procedure followed to find the dynamic features of the uncontrolled system is given. A short overview of the plant behavior in the sub-critical wind speed regime is presented, and finally the properties of the manifested stable LCO behavior are shown and discussed. Section 6.3 describes the closed-loop procedure and the results obtained with the hardware in the loop implemented controller, with attention on the novel architecture efficacy in damping flutter oscillations.

6.1 Aerodynamic Database

The static test has been mainly performed to validated CFD simulation results. This test has a twofold task: to verify the aerodynamic quality of the prototype and, primarily, to validate the aerodynamic database to test the control law design on a more realistic plant mathematical model. The *AEROLAB 5/8A* force/moment balance sting, used to perform the experiment, is equipped with a six-piezo sensor that, when deformed, returns different voltage in the order of magnitude of millivolt (mV). The electrical center of the balance sting is located at 3.525 inches (89.535 mm) from the forward tip, as shown in Figure 6.1. The balance measures moments about
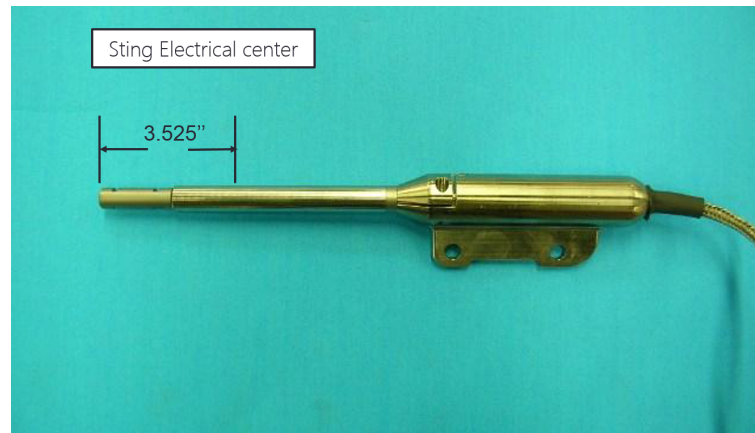
Figure 6.1: Aerolab 5/8-A force/moment sting

the electrical center. Knowing the indicated moment (as read by the data acquisition system) and the location of the electrical center of the balance, the moment about any other point can be determined. The sting balance calibration has been performed following the AIAA guidelines [95]. This process allows to read from a custom developed LabView code the output of the system in terms of: Normal Force, Side Force, Axial Force, Pitching Moment, Yawing Moment and Rolling Moment. Once stored in text files, the output are processed in *Matlab* to obtain the aerodynamic coefficient.

The test has been performed as follows:

- Calibration
  Known loads are used to obtain the calibration matrix that serves to convert voltages (V) to forces (N) and moment $(N \cdot m)$ values.

- Test article installation
  The wing section prototype is connected to the force balance sting, perfectly leveled with a laser pointer.

- Zero angle of attack
  Using a symmetric airfoil the aerodynamic zero angle of attack coincides with the zero pitch angle of the wing. It is verified both geometrically and aerodynamically.

- Zeroing forces and Baseline
  Starting from the zero pitch angle (equal to the AoA), the outputs are zeroed, and the baseline obtained. This consist in taking measurements, for the AoA's entire range of interest, of the wing at zero wind speed, allowing easy evaluation of the wing weight projection on the six components.

- Data Acquisition
  Turning on the fan so to reach the predefined wind speed of $U = 15(m/s)$, that means a Reynolds number of $Re \approx 3e^5$, the forces/moments measurements are acquired for each angle of attack, with steps of 1 degree, in the range of interest $\pm 18(deg)$ to include airflow separation. This process is repeated three times for each configuration, with increasing and decreasing trends of the angles of attack to stimulate and capture the hysteresis phenomenon due to airflow reattachment. Results are then averaged point by point. Six configurations total are analyzed: clean configuration first and then one to five open spoilers.

- Data post-processing
  The data read by the balance are expressed in the sting body axis, which means that they must be transformed to wing aerodynamic force by the following equations:

$$
\begin{aligned}
N(\theta_i) &= N_{measured}(\theta_i) - N_{Baseline}(\theta_i); \\
A(\theta_i) &= A_{measured}(\theta_i) - A_{Baseline}(\theta_i); \\
M(\theta_i) &= M_{measured}(\theta_i) - M_{Baseline}(\theta_i) - N_{measured}(\theta_i) \cdot l; \quad (6.1) \\
L(\theta_i) &= N(\theta_i) \cdot \cos(\theta_i) - A(\theta_i) \cdot \sin(\theta_i) \\
D(\theta_i) &= A(\theta_i) \cdot \cos(\theta_i) + N(\theta_i) \cdot \sin(\theta_i)
\end{aligned}
$$

where N and A are the normal and axial forces respectively, M is the pitching moment, L and D are lift and drag respectively, θ_i is the pitch angle at which the measurement has been taken, and l is the distance from the wing c.g. to the sting electric center. It is worth pointing out that the forces and moment in the lateral plane are null (or very close to zero) and not useful for the proposed research. Once the aerodynamic forces are determined, the coefficient are obtained by considering the actual atmospheric condition inside the room during the tests and the geometrical properties of the wing, by the standard formulation:

$$
\begin{aligned}
C_L(\theta_i) &= L(\theta_i)/qS; \\
C_D(\theta_i) &= D(\theta_i)/qS; \quad (6.2) \\
C_m(\theta_i) &= M(\theta_i)/qS\bar{c};
\end{aligned}
$$

where $q = 1/2\rho V^2$ is the dynamic pressure, S the wing surface and $\bar{c}$ its mean aerodynamic chord.

The aerodynamic coefficients are stored in a database and used in *Simulink* environment, in form of look-up table, in the wing simulation model as detailed in Chapter 2. The obtained database is reported hereafter in terms of the characteristic coefficients for the longitudinal plane: the lift curve is reported Figure 6.2, the pitching moment in Figure 6.3 and the polar in Figure 6.4. The results have been validated with CFD.
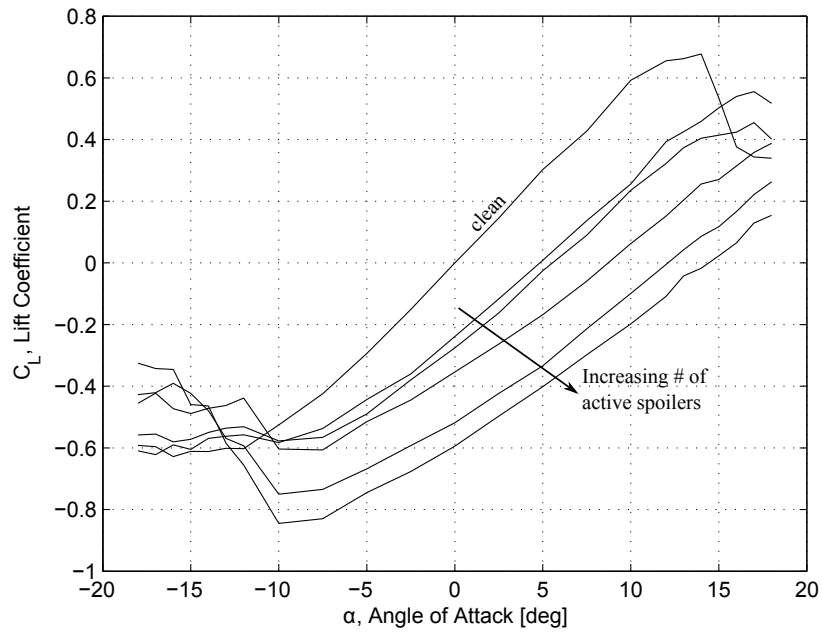
Figure 6.2: Wing-Spoiler configuration Aerodynamic Database, lift coefficient experimental values. Transition from clean to 5 open spoiler configuration is specified by the arrows
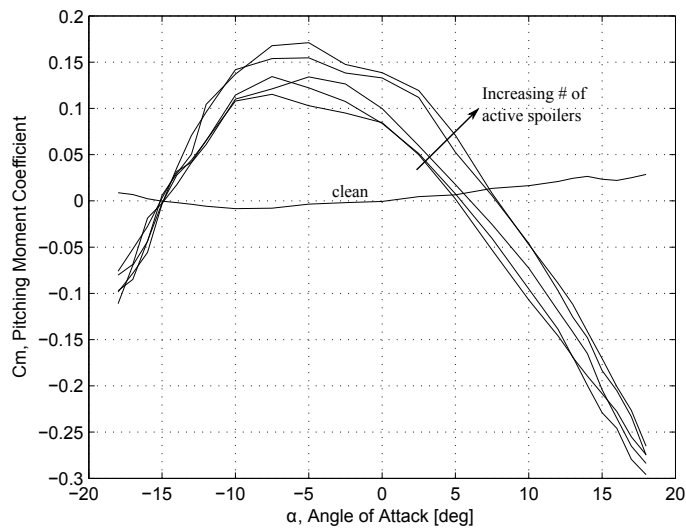

Figure 6.3: Wing-Spoiler configuration Aerodynamic Database, pitching moment coefficient experimental values. Transition from clean to 5 open spoiler configuration is specified by the arrows
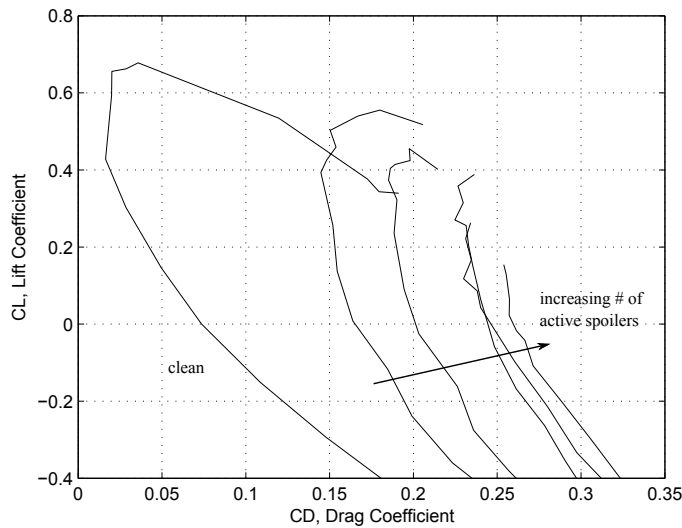
Figure 6.4: Wing-Spoiler configuration Aerodynamic Database, Polar. Transition from clean to 5 open spoiler configuration is specified by the arrows

6.2 Aeroelastic System Free Response

The aeroelastic properties of the prototyped wing-spoiler apparatus have been experimentally evaluated in the wind tunnel with the setup described in section 5.5. After the apparatus installation, but before activating the wind tunnel, all the instruments are checked for functioning, room atmospheric parameters are recored and the sensors calibration is verified. Flight flutter testing techniques are used to safely approach the open-loop flutter speed of the model based on its sub-critical response. The procedure implemented to investigate the free dynamic response of the wing is described hereafter, and depicted in the flow chart in Figure 6.5.

- Wind Tunnel ON
  Starting with the wing in resting position, all states are zero, the wind tunnel is activated to generate a wind speed of $U = 2(m/s)$. An extremely low wind speed is chosen for safety reason as flutter divergence can compromise the experiment. The Pitot probe is monitored to guarantee that stable wind speed is settled.

- Model Δh perturbation
  The system is perturbed in plunge from the resting position. The wing is positioned manually at the extreme end of the rail track, where the stopper are located, and held for seconds before being released.
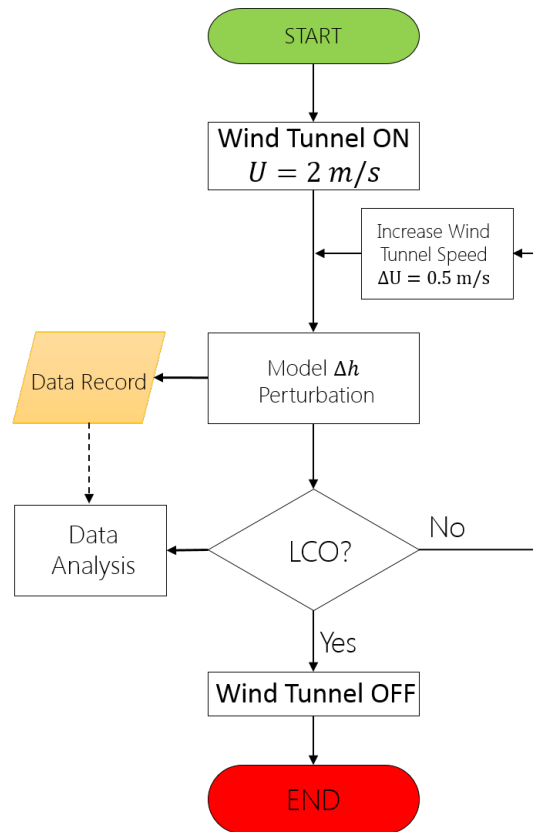
Figure 6.5: Open-Loop test flow chart

- System observation
  The system is then observed and the states monitored on the computer real time graphs. If the oscillations are quickly damped a higher increment of wind speed is given to the system (e.g. $\Delta U = 2(m/s)$). As the damping diminishes also the wind speed step is reduced down to $\Delta U = 0.5(m/s)$. This iterative process is continued until the occurrence of stable LCO.

- Data Recording and Analysis
  For the entire duration of the experiment data from sensors, plunge and pitch α, are monitored and recorded to be analyzed in post-process in terms of proper frequency, amplitude and damping of the wing section dynamic free response.

- Wind Tunnel OFF
  The experiments ends turning off the wind tunnel fan when sufficient information on the occurred dynamic motion have been acquired.

The most meaningful results, both in time and frequency domain, are shown next, from Figure 6.16 to Figure 6.17. The experimental campaign is primarily conducted without wind, at $U = 0(m/s)$, to investigate the proper modes of the wing-apparatus overall system. The free response test procedure is deductible form Figure 6.6a: the carriage is constrained manually at the rail track stopper and released after few seconds. This explains for the presence of the initial step in the plunge time history plot, $h(m)$. Through the several plots, the step has different duration and starts at different time instant because there is not any automatic mechanism for wing releasing. The manual system employed to perturb the wing is common practice and does not affect the quality of the test results. The wing motion is unaffected by the air until it reaches a speed of $U = 6(m/s)$, as reported in Table 6.1 and shown by the states PSD graphs (Figure 6.9). The system proper mode has a frequency of $2.051(Hz)$ in the pitch degree of freedom. The response to the perturbation remains unaltered both in time and in frequency domain for wind speed up to $U = 4(m/s)$. Higher wind speed induces a positive increment both in amplitude and frequency of the torsional mode. The plunging motion is highly damped and does not show any predominant mode until a wind speed of $U = 10(m/s)$ is reached (Figure 6.11). In this condition the system is approaching LCOs and the oscillation frequencies in the two degrees of freedom are converging to a unique value. The two motions' coupling, even for not self-sustained oscillations, occurs at a wind speed of $U = 10.5(m/s)$, with a coincident proper frequency of $2.588(Hz)$. The LCO regime starts at $U = 11(m/s)$ at a proper frequency of $2.686(Hz)$. It is characterized by bounded and self-sustained oscillations at a unique frequency for both plunging and pitching motion. For higher wind speed the two motions remain coupled and the oscillations' amplitude and frequency increase as expected. The experimental investigation terminates at a wind speed of $U = 15(m/s)$ when the plunge motion amplitude almost reaches the maximum allowed displacement by the carriage trail.

6.3 Aeroelastic System Closed-Loop Response

Once the uncontrolled motion dynamic features of the aeroelastic nonlinear system have been obtained and studied, a simple PID is implemented to control the plant. The model reference adaptive controller, developed on the simulation environment, has not been implemented because of the available hardware deficiency. The risk of not achieving real-time, could have compromised the entire experiment, damaging the installed apparatus and the wind tunnel itself. Hence, it has been decided to focus the attention on the verification of the aerodynamic efficacy of the spoilers' based actuation system. The implementation of a standard non-adaptive controller has been considered suitable for the actual scientific purpose. The PID controller is

Table 6.1: Experimental Wing Section Proper modes

Wind Speed $U(m/s)$	α PSD Peak (Hz)	h PSD Peak (Hz)
0	2.051	*n.d.*
2	2.051	*n.d.*
4	2.051	*n.d.*
6	2.148	*n.d.*
8	2.197	*n.d.*
10	2.539	*n.d.*
10.5	2.588	2.637
11	2.686	2.686
12	2.783	2.783
13	2.869	2.869
14	2.905	2.905
15	2.954	2.954
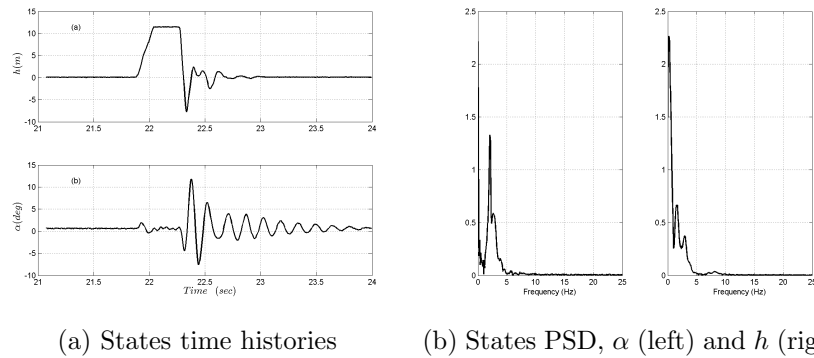
(a) States time histories   (b) States PSD, α (left) and h (right)

Figure 6.6: Wing free response. $U = 0(m/s)$
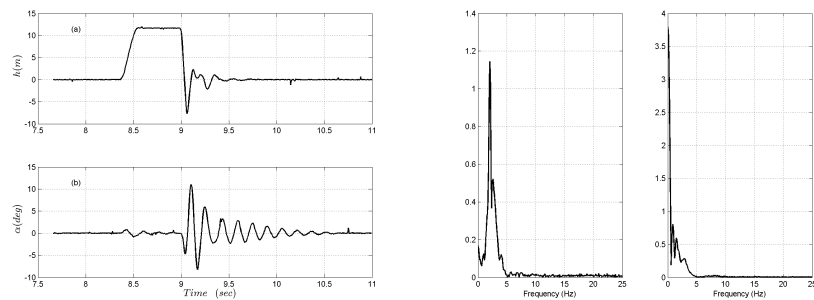
(a) States time histories   (b) States PSD, α (left) and h (right)

Figure 6.7: Wing free response. $U = 2(m/s)$

(a) States time histories

(b) States PSD, α (left) and h (right)

Figure 6.8: Wing free response. $U = 4(m/s)$

(a) States time histories

(b) States PSD, α (left) and h (right)

Figure 6.9: Wing free response. $U = 6(m/s)$

(a) States time histories

(b) States PSD, α (left) and h (right)
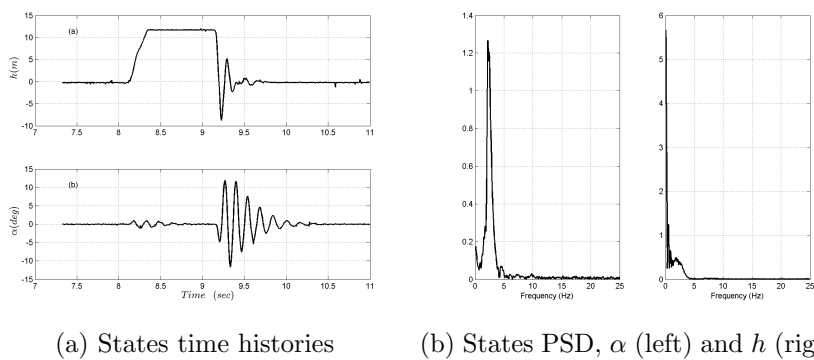
Figure 6.10: Wing free response. $U = 8(m/s)$

(a) States time histories   (b) States PSD, α (left) and h (right)
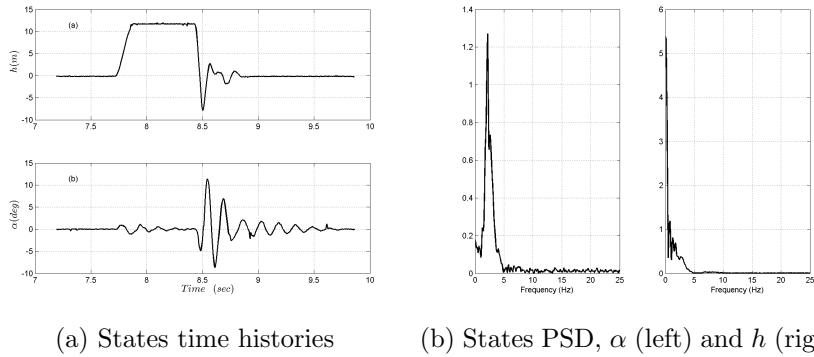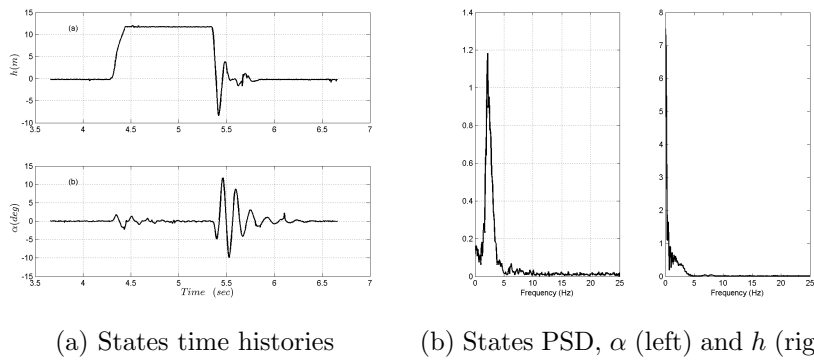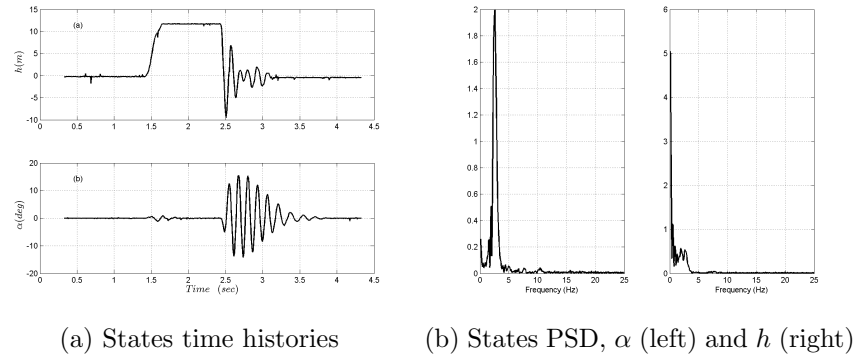
Figure 6.11: Wing free response. $U = 10(m/s)$

(a) States time histories   (b) States PSD, α (left) and h (right)
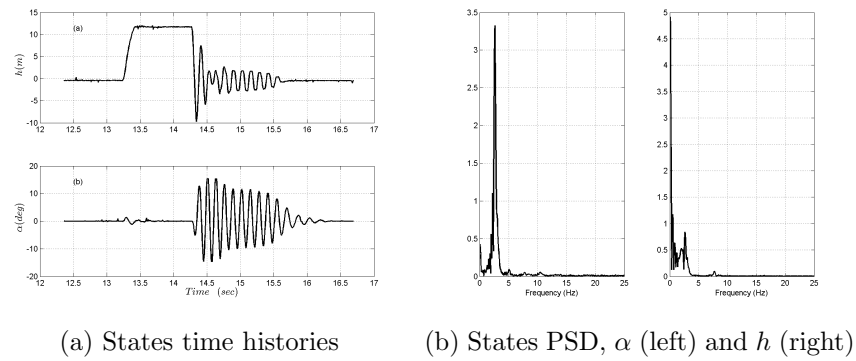
Figure 6.12: Wing free response. $U = 10.5(m/s)$

(a) States time histories   (b) States PSD, α (left) and h (right)

Figure 6.13: Wing free response. $U = 11(m/s)$

(a) States time histories   (b) States PSD, α (left) and h (right)
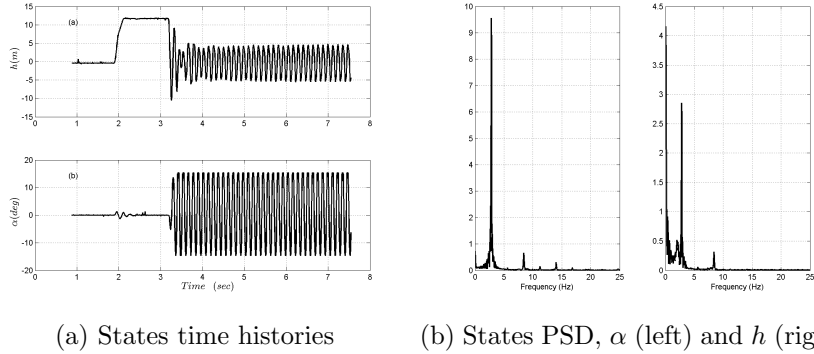
Figure 6.14: Wing free response. $U = 12(m/s)$

(a) States time histories   (b) States PSD, α (left) and h (right)
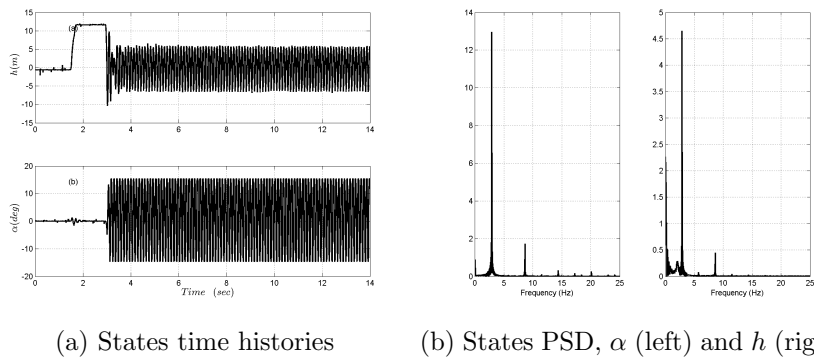
Figure 6.15: Wing free response. $U = 13(m/s)$

(a) States time histories   (b) States PSD, α (left) and h (right)
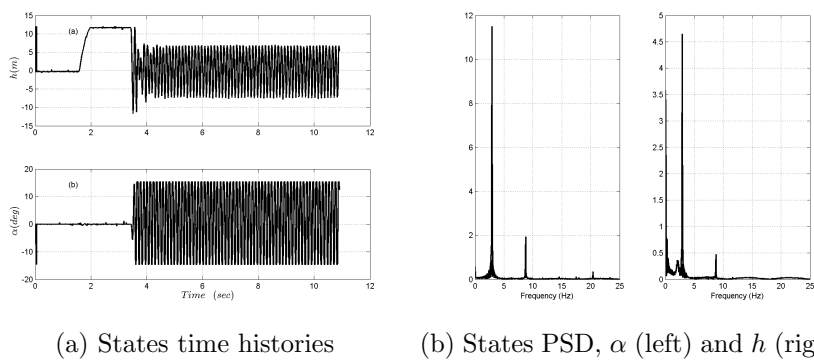
Figure 6.16: Wing free response. $U = 14(m/s)$

(a) States time histories   (b) States PSD, α (left) and h (right)
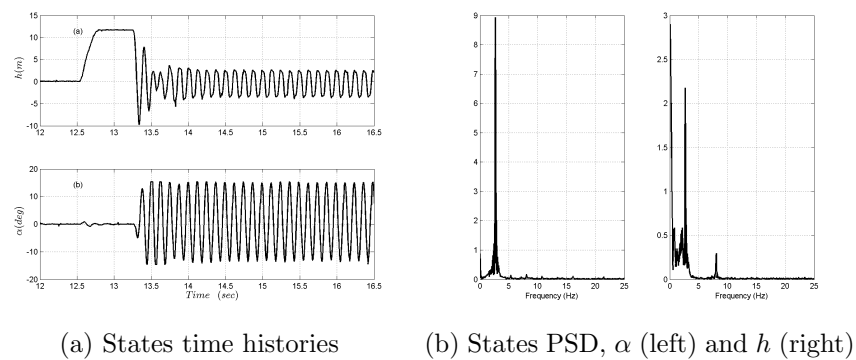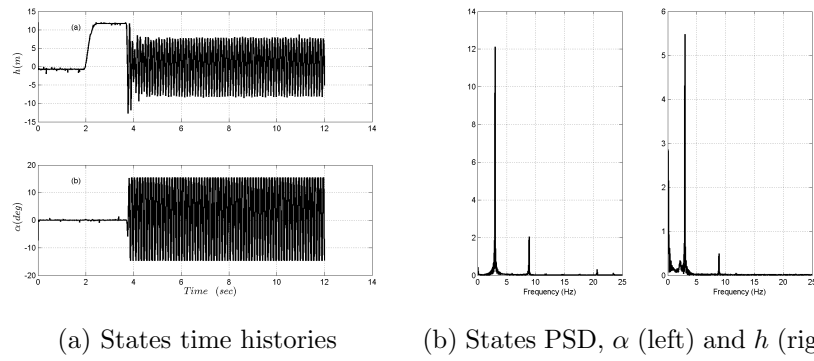
Figure 6.17: Wing free response. $U = 15(m/s)$

(a) Frequencies Trend   (b) Power Spectral Density Zoom
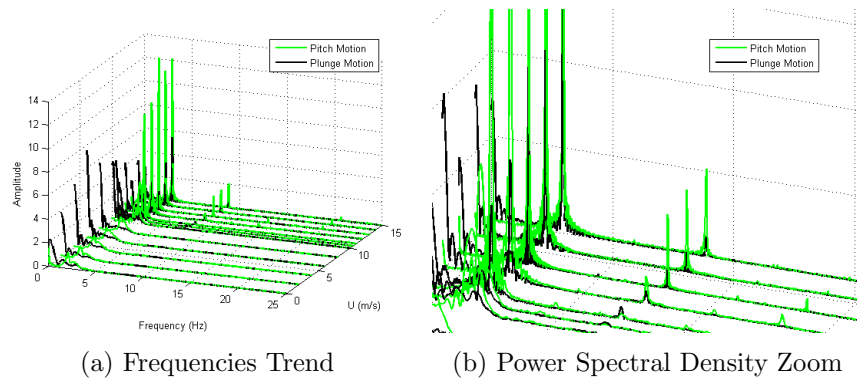
Figure 6.18: Wing Spoiler Experiment

implemented into the host computer using *Simulink* environment. The code returns an integer number within the range $[0-5]$, which is the $\#_{sp}$ to open. The link to the hardware is obtained through the Arduino board as explained in detail in Chapter 5. The PID gains are tuned by a standard iterative, trial and error, process. It is performed by exciting the system at the flutter speed $U = U_f$, as explained in Section 6.2, and activating the controller with LCO regime fully established. The dynamic response is monitored in terms of α, h and number of active spoilers $\#_{sp}$. The gain tuning process is continued until satisfying performances are met in terms of regulation time and steady-state error. Albeit both states, α and h, are accessible for measurements only the pitch angle is used as feedback signal to close the control loop. This choice has been made for sake of consistency with the simulation models, as explained in Chapters 2 and 3. In addition, the pitch signal is reliable and easy to be obtained, with dislocated accelerometers, in a real wing application. Two different types of closed-loop tests are conducted to verify the control architecture performance, as for the simulation models. First, the controller limitations are established by maintaining it active during the entire test duration. Impulsive perturbations in the plunge DOF are applied to the system at different wind speed. The first test procedure is shown in Figure 6.19, and consists of:

- Controller ON
  The system is connected to the hardware with the tuned PID controller active.

- Wind Tunnel ON
  The wind tunnel fan is activated at the predetermined *rpm* and the wind speed monitored to be $U = U_f$

- Model Δh perturbation
  The system is perturbed in plunge. Unlike the uncontrolled test, in this case an impulsive perturbation is given to the carriage to excite the LCOs.

- System observation
  The system dynamic response is observed monitoring its states on the computer real time diagrams. If the system is controlled with satisfactory performance in time domain an wind speed increment is applied $\Delta U = 0.5(m/s)$. This iterative process is continued until the control architecture demonstrates performance deterioration.

- Data Recording and Analysis
  For the entire duration of the experiment data from sensors, α, h, and the number of open spoilers ($\#_{sp}$) are monitored and recorded to be analyzed in post-process.

Figure 6.19: Closed-Loop test flow chart, perturbation with controller ON

- Wind Tunnel OFF
  The experiments ends deactivating the wind tunnel fan when sufficient information on the occurred dynamic motion have been acquired.

Once the control architecture capabilities have been explored, and the operative wind speed range identified, the second test is accomplished. In this case, the system dynamic is left free to fully develop into a stable LCO regime at the previous tested wind speed values. Subsequently, the controller is manually activated at a casual time. The second test procedure is shown in Figure 6.20 and consist of:

- Wind Tunnel ON
  The wind tunnel is activated at flutter speed.

- Model Δh perturbation
  The system is excited with an impulsive plunge perturbation while uncontrolled. Stable LCO regime is established.

- Controller ON
  The PID controller connected to the plant is activated.

- System observation
  The system dynamic response is observed monitoring its states on

Figure 6.20: Closed-Loop test flow chart, controller ON with LCO regime induced

the computer real time diagrams. If the system is controlled with satisfactory performance in time domain an wind speed increment is applied $\Delta U = 0.5(m/s)$. This iterative process is continued until the control architecture demonstrates performance deterioration.

- Data Recording and Analysis
  For the entire duration of the experiment data from sensors, α, h, and the number of open spoilers ($\#_{sp}$) are monitored and recorded to be analyzed in post-process.
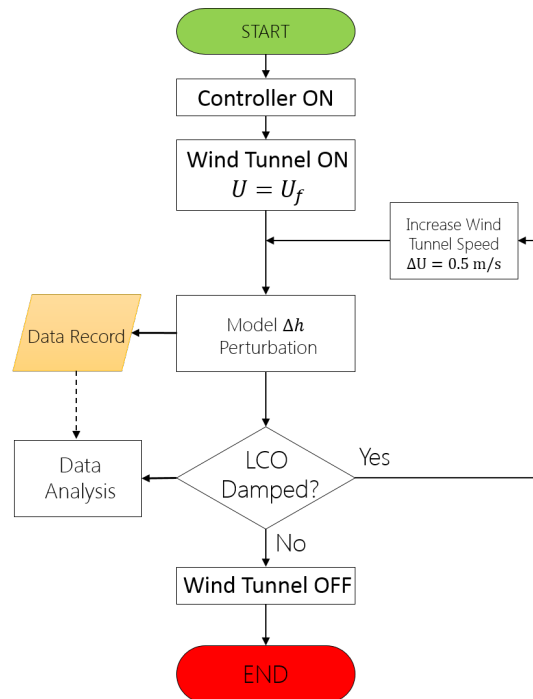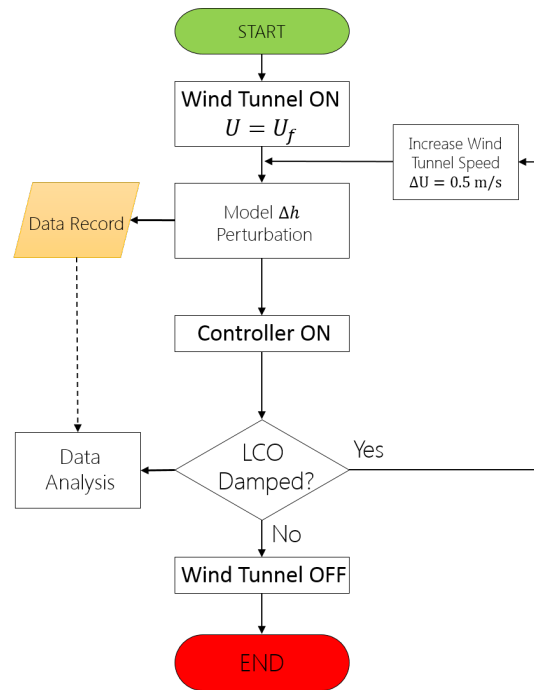
- Wind Tunnel OFF
  The experiments ends deactivating the wind tunnel fan when sufficient information on the occurred dynamic motion have been acquired.

Closed-loop experiment has been successfully performed as proven by the results shown next, from Figure 6.21 to Figure 6.23. The flutter suppression capabilities of the novel control architecture based on multiple distributed leading edge spoilers are proven. Flutter instabilities are controlled both from a resting initial condition and a from a developed LCO regime. The control system demonstrates better performance in the first case, showing noticeable results as far as a real-world application is concerned. In fact, the oscillations are damped out in $1.4(sec)$ precisely, when the aeroelastic

system is perturbed at flutter speed, $U = 11(m/s)$, with already active controller (Figure 6.21a). Whereas, slower response, about $2.5(sec)$, is detected when the controller is activated from the established LCO regime. The lag is caused by the kinetic energy that the system has acquired when already excited. This is critical for the spoiler actuation system because it works on one side only of the wing. Convergence to zero pitch angle and plunge is verified in both cases. In addition, the pre-designed spoilers' opening strategy demonstrated its efficacy during the experiment. The gradual and symmetric opening prevented any coupling with other undesired dynamics, guaranteeing pure pitching/plunging motion. The smooth and fast response obtained at the apparatus flutter speed experience performance deterioration at higher wind speed. In fact, at $U = 13(m/s)$ the control system exhibits a slightly slower response and higher peaks in α in general (Figure 6.22). More important, an unpredicted increase in the LCO frequency occurs before effectively appreciating damping in Figure 6.22b. This phenomenon is very fast and last for less than a second. The non-adaptive nature of the control law is the main cause of this behavior. The control action forces the nonlinear system to its own working frequency before properly interacting with it and damping out the oscillations. In fact, as summarized in Table 6.1, the wing pitch/plunge proper frequencies change as a function of U. On the contrary, the PID controller with constant gains works at a fixed bandwidth. The same behavior is detectable at wind speed $U = 15(m/s)$, shown inFigure 6.23. The actuation dynamics encounters difficulties to interact with the aeroelastic system until certain conditions are met and damping occurs. About $3(sec)$ are required to regulated the system both in Figure 6.23a and Figure 6.23b. The damping is not monotone but convergence is obtained in both cases. The ability of controlling the highly nonlinear aeroelastic system, in a real application, at a wind speed 36% higher of its flutter speed is a result of absolute importance. In particular, considering the non adaptive nature of the control law implemented, the efficacy of the spoiler-based control architecture can be considered successfully verified.
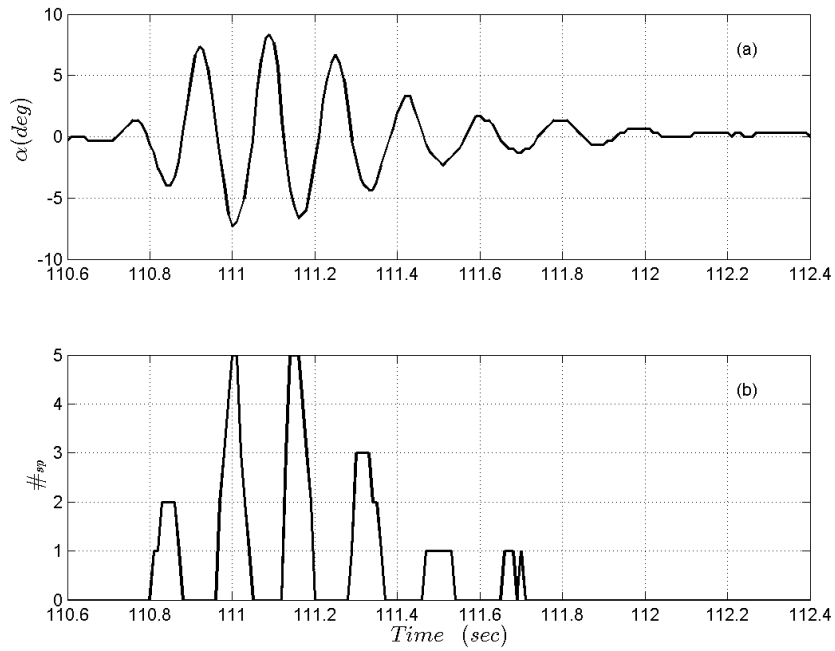
(a) Perturbation with active Controller
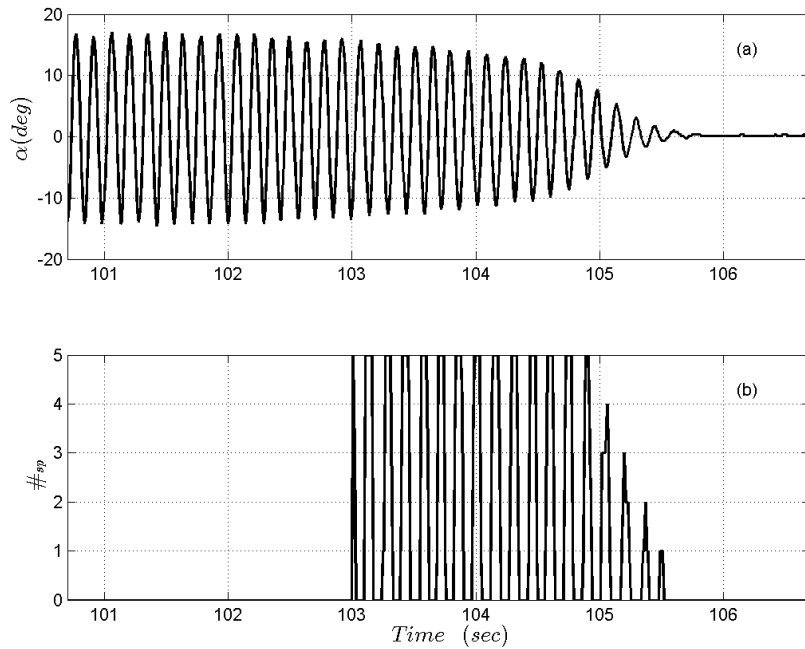
(b) Controller Activation with LCO established

Figure 6.21: Wing Spoiler Experiment,Closed loop Response at $U = 11(m/s)$

(a) Perturbation with active Controller

(b) Controller Activation with LCO established

Figure 6.22:   Wing Spoiler Experiment,Closed loop Response at $U = 13(m/s)$
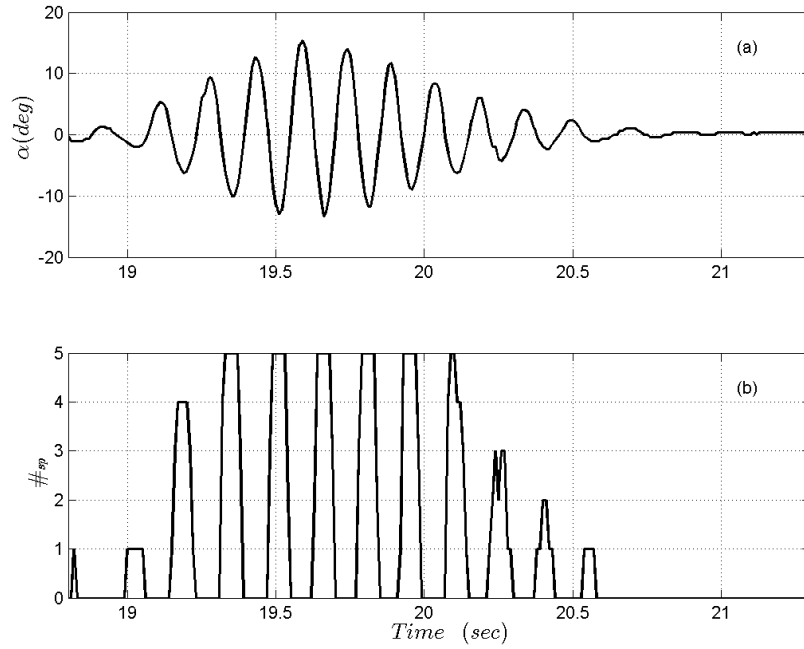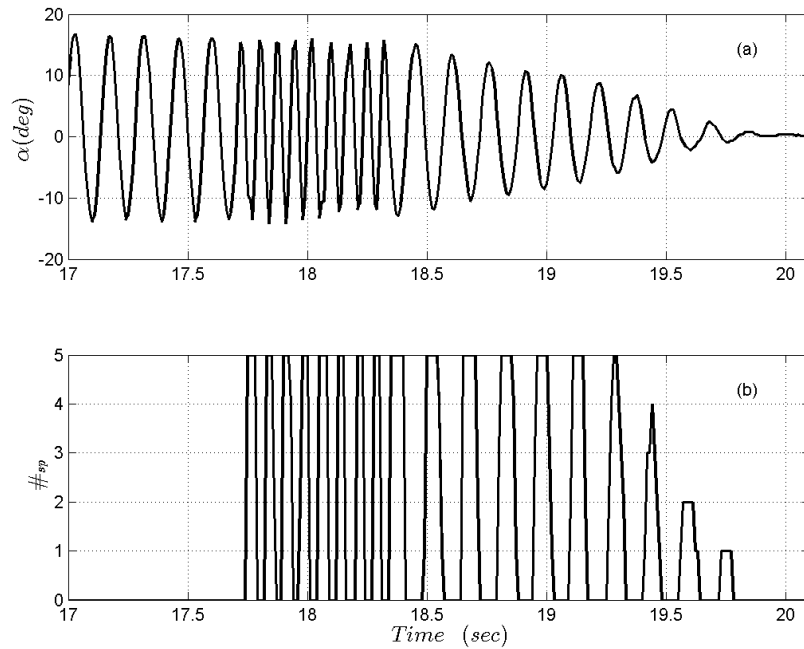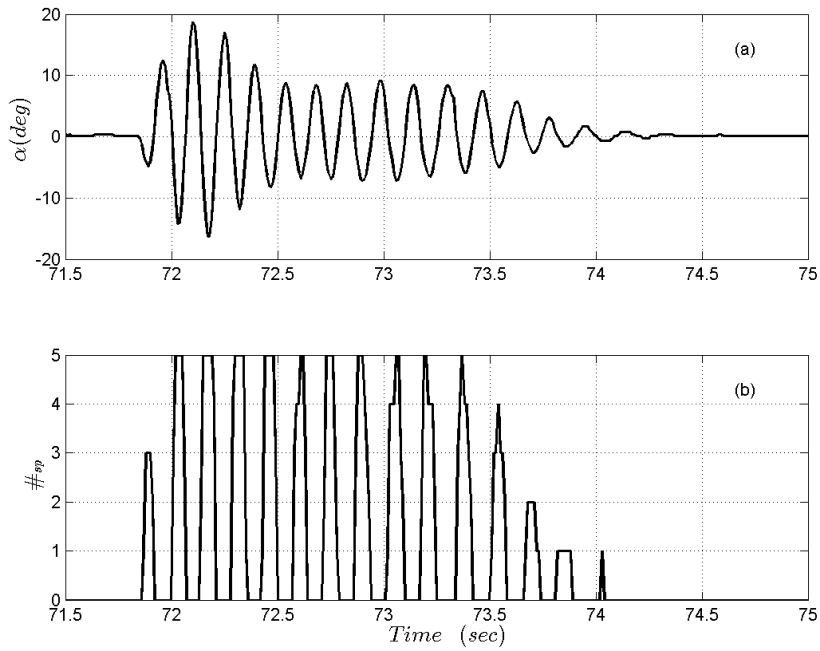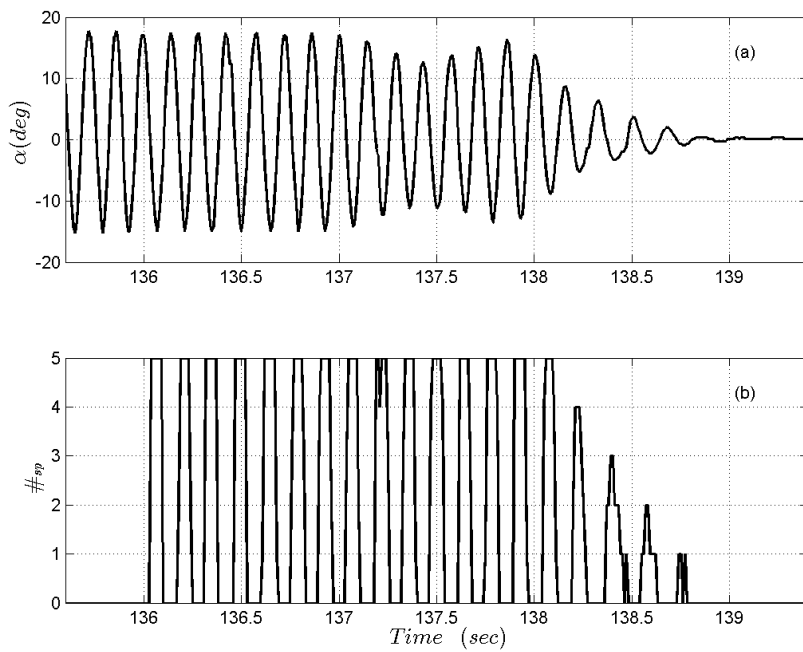
(a) Perturbation with active Controller

(b) Controller Activation with LCO established

Figure 6.23: Wing Spoiler Experiment,Closed loop Response at $U = 15(m/s)$

Chapter 7

Conclusion

This dissertation has focused on the modeling and control of nonlinear aeroelastic systems with different actuation strategies and different adaptive control algorithms. The techniques, employed for the control of the actuators, derive from recent studies on the performance and robustness improvement of model reference adaptive control scheme. In particular, emphasis is given to the derivation, implementation and performance analysis of four different adaptive control architectures: a Standard MRAC; a MRAC modified for performance improvement both in transient and steady tracking error, also called in the discussion *Modified MRAC*; a L_1 for systems with unknown constant parameters, called *Standard L_1*; and a L_1 for systems with uncertain system input gain, also called *Modified L_1*. None of this adaptive control schemes has never been derived or implemented for the bi-dimensional nonlinear aeroelastic model proposed, to the best of the author knowledge. Firstly, a standard 2D plunging/pitching aeroelastic system with trailing-edge control surface has been used as benchmark for control architectures performances and robustness testing purpose. Emphasis was placed on the definition of an effective methodology to evaluate the control schemes performance with respect to the nonlinear aeroelastic application. In fact, the application of external disturbances, consisting in different gusts profile that has been used as benchmark for controller's robustness comparison purpose, has been found to be a poor choice since also non-adaptive robust control law can tolerate a certain amount of external disturbances, however this fact does not make them adaptive controller. For this reason, an appropriate testing strategy has been developed considering a wider range of condition of critical interest from both an aeroelastic and a control point of view, such as post-flutter, stiffness reduction (simulating failure) and combined condition including gusts application. This new procedure, allowed a deep investigation of the different adaptive control schemes response and to obtain accurate comparison between them. This analysis aimed to choose the more robust and better performing architecture to be used with a novel

aeroelastic model, based on an wing section with a leading-edge multiple spoilers actuation strategy for flutter suppression, where the amount of uncertainties and unmodeled dynamics are significantly higher. A cross simulation/experimental approach has been used to design and verify the efficacy of the original control actuation architecture. In the dissertation, emphasis is given to the optimization process performed by CFD simulation to obtain the best spoiler configuration for maximizing positive pitching moment coefficient meanwhile reducing the detrimental effect of lag motion due to drag increment. Two different experimental campaign has been conducted for different purpose. First, on a wind tunnel six axis force balance, the leading-edge multiple spoilers actuation strategy effectiveness has been verified and the aerodynamic database obtained. Then, based on the experimental database, the mathematical model of the bi-dimensional plunging/pitching aeroelastic wing section with the novel actuation system has been derived and implemented in a simulation environment. A linearization methodology, commonly used in flight dynamic, has been applied to the system to evaluate each parameter effect on the oscillatory motion of the system. The control has been successfully obtained with the *Modified MRAC* scheme. This results has also been used to validate the control law robustness, being applied without modification from the trailing-edge flap application. The aeroelastic model derived served as reference to design and build the plunging/pitching experimental apparatus for testing of the real capabilities of the proposed actuation architecture in suppress flutter. The major outcomes of the presented research consist in an effective evaluation of the pros and cons of different model reference adaptive control schemes. Some examples are: a steady-state tracking error in the most critical conditions for the modified L_1 scheme, which reduces its adaptive capabilities; a residual oscillations propagation phenomenon due to the extremely high values of the adaptive gain which makes the adaptive law differential equation too stiff, in the standard L_1 scheme and makes the design of the filter a difficult and long process. Narrower filter bandwidth reduces oscillations but lead back to the steady-state tracking error effect, and the trade-off of the two is not an easy solution. In addition, slow adaptation is demonstrate for the *standard MRAC* scheme, that makes it not really suitable for aeroelastic application that works at higher frequencies than the model presented. The only scheme that have shown robust and fast enough response is the *Modified MRAC*, which indeed has been used for the multiple spoiler application. Other important findings concern the new spoiler-based actuation architecture, which has demonstrated encouraging performance in damping aeroelastic oscillations, so as to be considered a viable solution for real application as redundant or primary control system for flutter suppression.

Bibliography

[1] Curtiss H. C. Jr. Scanlan R. H. Dowell E. H. and F. Sisto. *A Modern Course in Aeroelasticity.* Kluwer Academic, Norwel, MA, 1989.

[2] Librescu L. Marzocca P. and G. Chiocchia. "Aeroelastic Response of a 2-D Lifting Surfaces to Gust and Arbitrary Explosive Loading Signatures". In: *International Journal of Impact Engineering* 25.1 (2001), pp. 41–65.

[3] Librescu L. Marzocca P. and G. Chiocchia. "Aeroelasticity of Two-Dimensional Lifting Surfaces via Indicial Function Approach". In: *Aeronautical Journal* 106.1056 (2002), pp. 147–153.

[4] Librescu L. 4. Marzocca P. and W. A. Silva. "Nonlinear Open-/Closed-Loop Aeroelastic Analysis of Airfoils via Volterra Series". In: *AIAA Journal* 42.4 (2004), pp. 673–686.

[5] N. Hovakimyan and C. Cao. *L1 Adaptive Control Theory, Guaranteed Robustness with Fast Adaptation.* SIAM, 2010.

[6] C. Cao and N. Hovakimyan. "L1 Adaptive Output Feedback Controller for Systems of Unknown Dimension". In: *IEEE Transactions on Automatic Control* 53.3 (2008), pp. 815–821.

[7] C. Cao and N. Hovakimyan. "Design and Analysis of a Novel L1 Adaptive Control Architecture with Guaranteed Transient Performance". In: *IEEE Transactions on Automatic Control* 53.2 (2008), pp. 586–591.

[8] Cao C. Kharisov E. Xargay E. Hovakimyan N. and I. Gregory. "L1 Adaptive Control for Safety-Critical Systems". In: *IEEE Control Systems Magazine* 31.5 (2011), pp. 54–104.

[9] Cestino E. Frulla G. Gerussi S. Gili P. Battipede M. "Innovative Aircraft Aeroelastic Modelling and Control". In: *27th Congress of the International Council of the Aeronautical Science 2010, ICAS2010* (2010), pp. 2321–2334.

[10] K.W. Lee and S.N. Singh. "L1 Adaptive Control of a Nonlinear Aeroelastic System Despite Gust Load". In: *Journal of Vibration and Control* 19.12 (2013), pp. 1807–1821.

[11] Marzocca P. Behal A. Cassaro M. Battipede M. "Comparison of Adaptive Control Architectures for Flutter Suppression". In: *Journal of Guidance, Control, and Dynamics* 38.2 (2015), pp. 346–355.

[12] Mancini A. R. Aseltine J. A. and C. W. Sartune. "A Survey of Adaptive Control Systems". In: *IRE Transactions on Automatic Control* 3.6 (1958), pp. 102–108.

[13] W.I. Caldwell. "Control System with Automatic Response Adjustment". In: *American patent, 2,517,081.* (1950).

[14] I. Ashkenas McRuer D. and D. Graham. *Aircraft Dynamics and Automatic Control.* Princeton, New Jersey: Princeton University Press, 1973.

[15] Gili P. Gunetti P. Battipede M. Cassaro M. "Modeling and validation of aircraft mathematical models for the development of an innovative Flight Management System". In: *CEAS 2011 The International Conference of the European Aerospace Societies* Venice ().

[16] M. Cassaro. *Modeling and validation of a B747-100 AFCS suite for the development of an innovative Flight Management System.* Turin: Master Thesis, Politecnico di Torino, 2011.

[17] A.P. Whitaker Osburn P.V. and A. Kezer. "New Developments in the Design of Model Reference Adaptive Control Systems". In: *Institute of the Aerospace Sciences* (1961).

[18] J. Yamron Whitaker H.P. and A. Kezer. "Design of Model Reference Adaptive Control Systems for Aircraft". In: *Report R-164, Instrumentation Laboratory, M. I. T. Press, Cambridge, Massachusetts* (1958).

[19] R.E. Kalman. "Design of a Self Optimizing Control System". In: *Transaction of the ASME* 80 (1958), pp. 468–478.

[20] K.J. Astrom. "Theory and Applications of Adaptive Control-A Survey". In: *Automatica* 19.5 (1983), pp. 471–486.

[21] L.W. Taylor and E.J. Adkins. "Adaptive Control and the X-15". In: *Proceedings of Princeton University Conference on Aircraft Flying Qualities* (1965).

[22] R.E. Bellman. *Dynamic Programming.* Princeton, New Jersey: Princeton University Press, 1957.

[23] R.E. Bellman. *Adaptive Control Processes-A Guided Tour.* Princeton, New Jersey: Princeton University Press, 1961.

[24] A.A. Fel'dbaum. *Optimal Control Systems.* New York: Academic Press, 1965.

[25] K.J. Astrom and P. Eykhoff. "System Identification-A Survey". In: *Automatica* 7 (1971), p. 123.

[26] Y.Z. Tsypkin. "Adaptation and Learning in Automatic Systems". In: *Academic Press* (1971).

[27] B. Egardt. *Stability of Adaptive Controllers*. Vol. 20. Berlin: Lecture Notes in Control and Information Sciences, Springer-Verlag, 1979.

[28] A.S. Morse. "Global Stability of Parameter Adaptive Control Systems". In: *IEEE Transactions on Automatic Control* 25 (1980), pp. 433–439.

[29] Y.H. Lin Narendra K.S. and L.S. Valavani. "Stable Adaptive Controller Design, Part II: Proof of Stability". In: *IEEE Transactions on Automatic Control* 25.3 (1980), pp. 440–448.

[30] I.D. Landau. *Adaptive Control: The Model Reference Approach*. New York: Marcel Dekker, Inc., 1961.

[31] P.J. Ramadge Goodwin G.C. and P.E. Caines. "Discrete-Time Multivariable Adaptive Control". In: *IEEE Transactions on Automatic Control* 25.3 (1980), pp. 449–456.

[32] G.C. Goodwin and K.C. Sin. *Adaptive Filtering Prediction and Control*. New Jersey: Prentice Hall, Englewood Cliffs, 1984.

[33] C.J. Harris and S.A. Billings. *Self-Tuning and Adaptive Control: Theory and Applications*. London: Peter Peregrinus, 1981.

[34] K.S. Narendra and R.V. Monopoli. *Applications of Adaptive Control*. New York: Academic Press, 1980.

[35] H. Unbehauen. *Methods and Applications in Adaptive Control*. Berlin: Springer-Verlag, 1980.

[36] P.A. Ioannou and P.V. Kokotovic. *Adaptive Systems with Reduced Models*. New York: Lecture Notes in Control and Information Sciences, Vol. 47, Springer-Verlag, 1983.

[37] L. Valavani M. Athans Rohrs C.E. and G. Stein. "Robustness of Continuous-time Adaptive Control Algorithms in the Presence of Unmodeled Dynamics". In: *IEEE Transactions on Automatic Control* 30.9 (1985), pp. 881–889.

[38] P.A. Ioannou and J. Sun. "Theory and Design of Robust Direct and Indirect Adaptive Control Schemes". In: *Int. Journal of Control* 47.3 (1988), pp. 775–813.

[39] P.A. Ioannou and A. Datta. "Robust Adaptive Control: Design, Analysis and Robustness Bounds". In: *Grainger Lectures: Foundations of Adaptive Control* (1991).

[40] Tsakalis K.S. and P.A. Ioannou. *Linear Time Varying Systems: Control and Adaptation*. New Jersey: Prentice Hall, Englewood Cliffs, 1993.

[41] I. Kanellakopoulos. *Adaptive Control of Nonlinear Systems*. Urbana, IL 61801.: Ph.D Thesis, Report No. UIUC-ENG-91-2244, DC-134, University of Illinois at Urbana-Champaign, Coordinated Science Lab.

[42] P.V. Kokotovic Kanellakopoulos I. and A.S. Morse. "Systematic Design of Adaptive Controllers for Feedback Linearizable Systems". In: *IEEE Transactions on Automatic Control* 36 (1991), pp. 1241–1253.

[43] A. Datta and P.A. Ioannou. "Performance Improvement Versus Robust Stability in Model Reference Adaptive Control". In: *Proceedings of the 30th IEEE Conference on Decision and Control* (1991), pp. 1082–1087.

[44] J. Sun. "A Modified Model Reference Adaptive Control Scheme for Improved Transient Performance". In: *Proceedings of 1991 American Control Conference* (1991), pp. 150–155.

[45] C. Cao and N. Hovakimyan. "Stability Margins of L1 Adaptive Control Architecture". In: *IEEE Transactions on Automatic Control* 55.2 (2010), pp. 480–487.

[46] Dobrokhodov V. Kaminer-I.-Hovakimyan-N. Cao-C. Gregory I. M. Xargay E. and R. B. Statnikov. In: *Proc. AIAA Guidance, Navigation and Control Conf.* AIAA-2010-7773 (2010).

[47] Y. C. Fung. *An introduction to the Theory of Aeroelasticity*. Dover, New York, 1989.

[48] Ashley H. Bisplinghoff R. L. and R. L. Halfman. *Aeroelasticity*. New York: Dover, 1996.

[49] A. H. Nayfeh and D. T. Mook. *Nonlinear Oscillations*. New York: Wiley, 1979.

[50] S. R. Cole. "Effects of Spoiler Surfaces on the Aeroelastic Behavior of a Low-Aspect Ratio Wing". In: *Proceedings of the AIAA 31st Structures, Structural Dynamics, and Materials Conference* (1990), pp. 1455–1463.

[51] Runyan H. L. Woolston D. S. and R. E. Andrews. "An Investigation of Effects of Certain Types of Structural Nonlinearities on Wing and Control Surface Flutter". In: *Journal of the Aeronautical Sciences* 24.1 (1957), pp. 57–63.

[52] E. J. Breitbach. "Flutter Analysis of an Airplane with Multiple Structural Nonlinearities in the Control System". In: *NASA TP 1620* ().

[53] E. Breitbach. "Effects of Structural Nonlinearities on Aircraft Vibration and Flutter". In: *AGARD-R-665* ().

[54] B. H. K. Lee and J. Desrochers. "Flutter Analysis of a Two-Dimensional Airfoil Containing Structural Nonlinearities". In: *Aeronautical Rept. LR-618* 27833 (1987).

[55] Alighanbari H. Price S. J. and B. H. K. Lee. "Postinstability Behavior of a Two-Dimensional Airfoil with a Structural Nonlinearity". In: *Journal of Aircraft* 31.6 (1994), pp. 1395–1401.

[56] Strganac T. W. Gilliatt-H. C. O'neil T. "Investigations of Aeroelastic Response for a System with Continuous Structural Nonlinearities". In: *AIAA Paper* 96.1390 ().

[57] Strganac T. W. O'neil T. "Nonlinear Aeroelastic Response-Analyses and Experiments". In: *AIAA Paper* 96.0014 ().

[58] Strganac T. W. O'neil T. "Aeroelastic Response of a Rigid Wing Supported by Nonlinear Springs". In: *Journal of Aircraft* 35.4 ().

[59] Laurenson R. M. Eversman-W. Galecki G.-Qumei I. Hauenstein J. and A. K. Amos. "Chaotic Response of Aerosurfaces with Structural Nonlinearities". In: *Proceedings of the AIAA 31st Structures, Structural Dynamics, and Materials Conference* ().

[60] Z. C. Yang and L. C. Zhao. "Analysis of Limit Cycle Flutter of an Airfoil in Incompressible Flow". In: *Journal of Sound and Vibration* 23.1 (1998), pp. 1–13.

[61] D. M. Tang and E. H. Dowell. "Comparison of Theory and Experiment for Non-Linear Flutter and Stall Response of a Helicopter Blade". In: *Journal of Sound and Vibration* 165.2 (1993), pp. 251–276.

[62] Strganac T. W.-Harrand V. J.-Thompson E. D. Sheta E. F. "Computational and Experimental Investigation of Limit Cycle Oscillations of Nonlinear Aeroelastic Systems". In: *Journal of Aircraft* 39.1 ().

[63] L. Meirovitch. *Methods of Analytical Dynamics*. New York: McGraw Hill, 1970.

[64] T. Theodorsen. "General Theory of Aerodynamic Instability and the Mechanism of Flutter". In: *NACA Report* 496 (1935).

[65] Strganac T. W. Kurdila-A. J. Ko J. "Stability and Control of a Structurally Nonlinear Aeroelastic System". In: *Journal of Guidance, Control, and Dynamics* 21.5 (1998), pp. 718–725.

[66] Kurdila A. J. Ko J. and T.W. Strganac. "Nonlinear Control of a Prototypical Wing Section with Torsional Nonlinearity". In: *Journal of Guidance, Control, and Dynamics* 20.6 (1997), pp. 1181–1189.

[67] D. J. Jones and B. H. K. Lee. "Time Marching Numerical Solution of the Dynamic Response of Nonlinear Systems". In: *National Aeronautical Establishment* Aeronautical Note.25 (1985).

[68] M. Karpel. "Design for Active Flutter Suppression and Gust Alleviation Using State-Space Aeroelastic Modeling". In: *Journal of Aircraft* 19.3 (1982), pp. 221–227.

[69]   M.R. Waszak. "Robust Multivariable Flutter Suppression for Bench-
        mark Active Control Technology Wind-Tunnel Model". In: *Journal of
        Guidance, Control, and Dynamics* 24.1 (2001), pp. 147–153.

[70]   A.G. Kelkar and S.M. Joshi. "Passivity-Based Robust Control with
        Application to Benchmark Controls Technology Wing". In: *Journal of
        Guidance, Control, and Dynamics* 23.5 (2000), pp. 938–947.

[71]   V. Mukhopadhyay. "Transonic Flutter Suppression Control Law De-
        sign and Wind-Tunnel Test Results". In: *Journal of Guidance, Con-
        trol, and Dynamics* 23.5 (2000), pp. 930–937.

[72]   J.J. Block and T.W. Strganac. "Applied Active Control for a Non-
        linear Aeroelastic Structure". In: *Journal of Guidance, Control, and
        Dynamics* 21.6 (1998), pp. 838–845.

[73]   G. Platanitis and T.W. Strganac. "Control of a Nonlinear Wing Sec-
        tion Using Leading- and Trailing-Edge Surfaces". In: *Journal of Guid-
        ance, Control, and Dynamics* 27.1 (2004), pp. 52–58.

[74]   G. Platanitis and T.W. Strganac. "Suppression of Control Reversal
        Using Leading- and Trailing-Edge Control Surfaces". In: *Journal of
        Guidance, Control, and Dynamics* 28.3 (2005), pp. 452–460.

[75]   Singh S.N. Yim W. Gujjula S. "Adaptive and Neural Control of a Wing
        Section Using Leading- and Trailing-Edge Surfaces". In: *Aerospace
        Science and Technology* 9.2 (2005), pp. 161–171.

[76]   Marzocca P. Rao V.M.-Gnann A. Behal A. "Nonlinear Adaptive Con-
        trol of an Aeroelastic Two-Dimensional Lifting Surface". In: *Journal
        of Guidance, Control, and Dynamics* 29.2 (2006), pp. 382–390.

[77]   Bliss D. B. Dowell E. H. and R. L. Clark. "Aeroelastic Wing with
        Leading- and Trailing-Edge Control Surfaces". In: *Journal of Aircraft*
        40.3 (2003), pp. 559–565.

[78]   R. V. Jr. Doggett. "Some Effects of Aerodynamic Spoilers on Wing
        Flutter". In: *NASA Technical Memorandum* 101632 ().

[79]   Rohcs J. Rgert T. Nagy A. "Investigation On The Effect Of Hydro-
        dynamic Mems On Airfoil". In: *ICAS2008* 3.10 (2008).

[80]   H. Wagner. "Uber die Entstehung des dynamischen Auftriebes von
        Tragflugeln". In: *Zeitschrift fur Angewandte Mathematic und Mechanik*
        5.1 (1925), pp. 17–35.

[81]   Nordwall D.R. Hanke C.R. "The Simulation of a Jumbo Jet Transport
        Aircraft". In: *The Boeing Company, Wichita Division* 2.D6-30643 ().

[82]   Behal A. Wang Z. and P. Marzocca. "Model-Free Control Design
        for Multi-Input Multi-Output Aeroelastic System Subject to Exter-
        nal Disturbance". In: *Journal of Guidance, Control, and Dynamics*
        34.2 (2011), pp. 446–458.

[83] Keum W. Lee and Sahjendra N. Singh. "Robust Higher-Order Sliding-Mode Finite-Time Control of Aeroelastic Systems". In: *Journal of Guidance, Control, and Dynamics* 37.5 (2014), pp. 1664–1671.

[84] Keum W. Lee and Sahjendra N. Singh. "Multi-Input Higher-order Sliding Mode Control of Aeroelastic Systems With Uncertainties and Gust Load". In: *AIAA Guidance, Navigation, and Control Conference* (2014).

[85] S.N. Singh and L. Wang. "Output Feedback Form and Adaptive Stabilization of a Nonlinear Aeroelastic System". In: *Journal of Guidance, Control, and Dynamics* 25.4 (2002), pp. 725–732.

[86] J.W. Edwards. "Unsteady Aerodynamic Modeling and Active Aeroelastic Control". In: *NASA CR* 148019 (1977).

[87] P.A. Ioannou and J. Sun. *Robust Adaptive Control.* New York: Dover, 2012.

[88] Lewis F. L. Stevens B. L. *Aircraft Control and Simulation.* Jhon Wiley & Sons, Inc., 1992.

[89] S. H. Lehnigk. *On the Hurwitz matrix.* Zeitschrift fr Angewandte Mathematik und Physik (ZAMP).

[90] Petros A. I. Datta A. "Performance Analysis and Improvement in Model Reference Adaptive Control". In: *IEEE Transactions on Automatic Control* 39.12 ().

[91] Petros A. I. Rudd L. Jafari S. "What is L1 Adaptive Control". In: *AIAA Guidance, Navigation, and Control (GNC) Conference* ().

[92] Cestino E. Marzocca P. Behal A. Cassaro M. Battipede M. "L_1 adaptive flutter suppression control strategy for highly flexible structure". In: *Sae International Journal of Aerospace* 6 (2013).

[93] K. Pooya. "Active Flow Control over a NACA 0015 Airfoil by Synthetic Jet Actuators". In: *Ph.D. Dissertation, Clarkson University* ().

[94] C. D. Hoover. *Design and Experimentation of a Flutter-Like Aeroelastic Power Source-Flaps.* Clarkson Univerisity, Master Thesis, 2008.

[95] AIAA R-091-2003. *Calibration and Use of Internal StrainGage Balances with Application to Wind Tunnel Testing.* American Institute of Aeronautics and Astronautics, 2003.

[96] W. Xing and S.N. Singh. "Adaptive Output Feedback Control of a Nonlinear Aeroelastic Structure". In: *Journal of Guidance, Control, and Dynamics* 23.6 (2000), pp. 1109–1116.

[97] Pado-L.E. Scott R.C. "Active Control of Wind-Tunnel Model Aeroelastic Response Using Neural Networks". In: *Journal of Guidance, Control, and Dynamic* 23.6 (2000), pp. 1100–1108.

[98] Ko-J. Thompson D.E. Kurdila A.J. Strganac T.W. "Identification and Control of Limit Cycle Oscillations in Aeroelastic Systems". In: *Journal of Guidance, Control, and Dynamic* 23.6 (2000), pp. 1127–1133.

[99] R.K. Prasanth and R.K. Mehra. "Control of a Nonlinear Aeroelastic System Using EulerLagrange Theory". In: *Journal of Guidance, Control, and Dynamic* 23.6 (2000), pp. 1134–1139.

**COMMISSIONE GIUDICATRICE
"INGEGNERIA AEROSPAZIALE"**

Il dott. CASSARO Mario ha discusso in data 30 aprile 2015 presso il Dipartimento di Ingegneria Meccanica e Aerospaziale del Politecnico di Torino la tesi di Dottorato avente il seguente titolo:

Model Reference Adaptive Control Laws: Application to Nonlinear Aeroelastic Systems

Le ricerche oggetto della tesi sono pertinenti con il profilo richiesto per un Dottore di ricerca in Ingegneria Aerospaziale

Le metodologie appaiono multidisciplinari, presentando aspetti teorici, numerici e sperimentali. Alcuni aspetti sperimentali costituiscono spunti da approfondire per meglio sostenere la generalità delle tesi presentate.

I risultati presentati sono interessanti ed analizzati con apprezzabile senso critico.

Nel colloquio il candidato dimostra una buona padronanza degli argomenti affrontati e consapevolezza dei limiti e delle potenzialità delle tematiche trattate.

La Commissione unanime giudica ottimo il lavoro svolto e propone che al dott. CASSARO Mario venga conferito il titolo di **Dottore di Ricerca**.

Data, 30 aprile 2015

Prof. Mauro VELARDOCCHIA (Presidente)

Prof. Giuseppe SALA (Componente)

Prof. Franco BERNELLI ZAZZERA (Segretario)